Catalytic selective oxidation of isobutane in a decoupled redox-process

Li Zhang, Jérémie Zaffran, Franck Dumeignil, Sébastien Paul, Axel Löfberg, Benjamin Katryniok

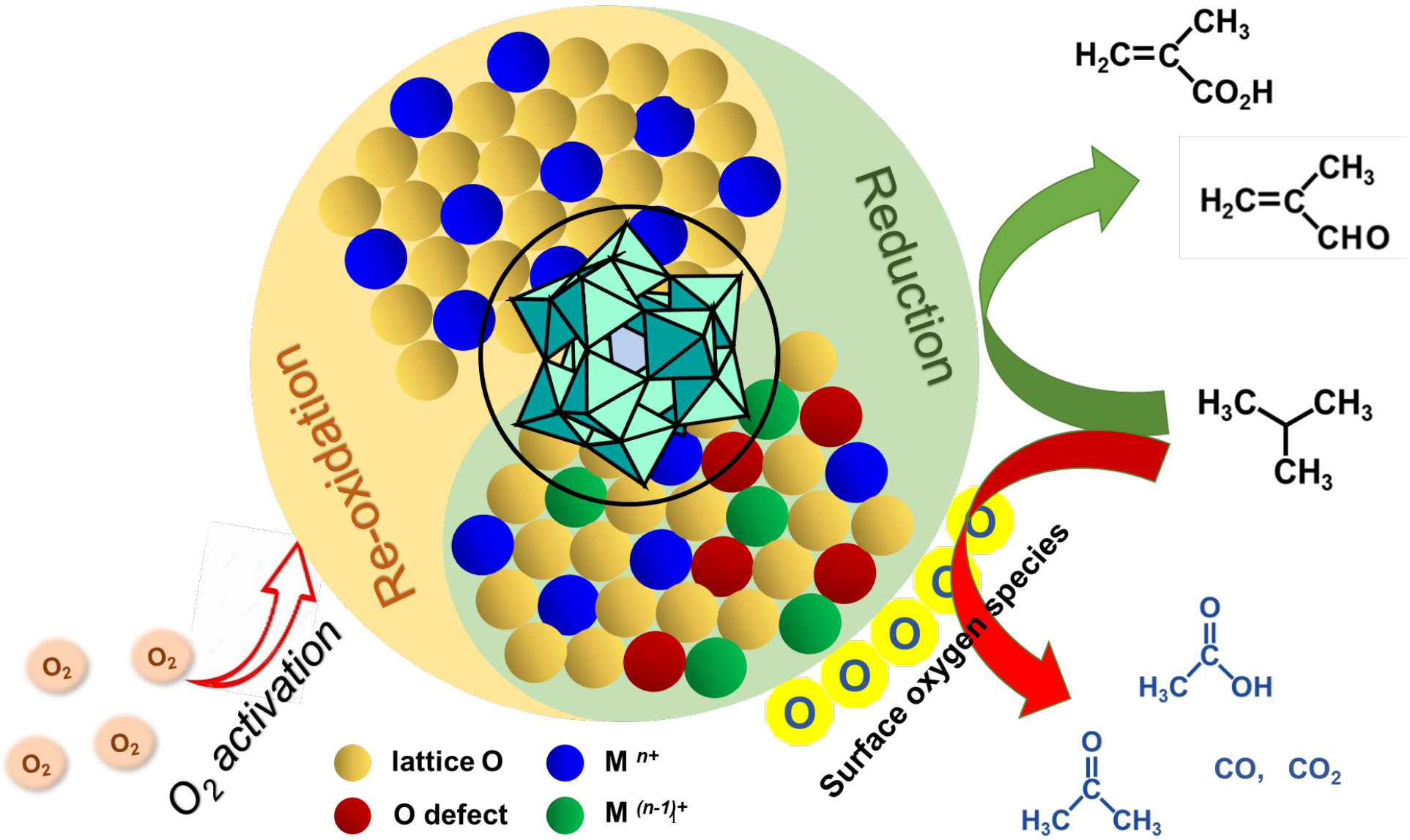
Re-oxidation
Reduction
O_2 activation
O_2
O_2
O_2
O_2
lattice O
O defect
M $^{n+}$
M $^{(n-1)+}$
Surface oxygen species
O
O
O
O
O
$H_2C=C(CH_3)CO_2H$
$H_2C=C(CH_3)CHO$
$H_3C-C(CH_3)_2-CH_3$
$H_3C-C(=O)-OH$
$H_3C-C(=O)-CH_3$
CO, CO_2

Catalytic selective oxidation of *iso*butane in a decoupled redox-process

Li Zhang, Jérémie Zaffran, Franck Dumeignil, Sébastien Paul*, Axel Löfberg,

Benjamin Katryniok*

[a] *Univ. Lille, CNRS, Centrale Lille, Univ. Artois, UMR 8181 – UCCS – Unité de Catalyse et Chimie du Solide, F-59000 Lille, France*

***** Corresponding authors: Sébastien Paul, sebastien.paul@centralelille.fr, Benjamin Katryniok, benjamin.katryniok@centralelille.fr

Abstract

The catalytic selective oxidation of *iso*butane to methacrolein (MAC) and methacrylic acid (MAA) is known to proceed via a Mars-Van Krevelen mechanism. When the reaction is performed in a common reactor with co-feeding of the reactant and oxygen, reactive oxygen species are present on the catalyst surface whereby non-selective oxidation reactions occur. In this work, we studied the possibility to decouple the redox mechanism meaning to separate the reactant oxidation step and the catalyst re-oxidation step for the selective oxidation of *iso*butane (IBAN) to MAC and MAA. For this purpose, two reactor configurations were employed: a periodic reactor and a two-zone fluidized bed reactor (TZFBR). Whereas the periodic reactor allows the temporal separation of the two steps, the TZFBR enables the spatial separation.

A Cs-based Keggin type heteropolycompound was employed as catalyst and characterized before and after reaction by XRD, Raman and XPS to better understand the structural and chemical changes during the periodic operation. The effect of the oxygen/IBAN concentration on the performance was studied. For the periodic reactor it was found that the conversion of *iso*butane and the formation of products decreased with the consumption of available oxygen species in the catalyst during a period. For the whole periodic tests, low concentration of oxygen injected into the reoxidation part of the cycles led to a high selectivity to the desired products (MAC+MAA).

Keywords: Keggin-type HPA, *iso*butane, heterogeneous catalysis, decoupled redox-process

1. Introduction

The selective oxidation of *iso*butane (IBAN) to methacrolein (MAC) and methacrylic acid (MAA) has attracted considerable interest over the last few decades as it is a one-step route to form MAA avoiding environmental problems associated with the currently used acetone cyanohydrin process [1–5]. However, the selective oxidation of IBAN remains challenging due to *i)* the activation of the very stable C-H bond and *ii)* the control of the oxidation reactions to selectively obtain the desired products.

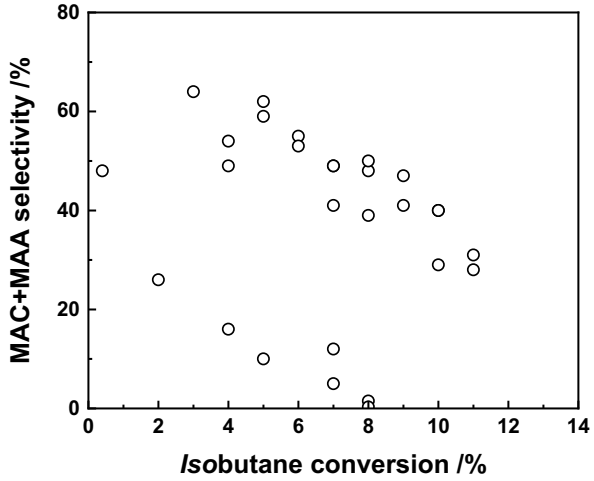

Fig. 1. MAC+MAA selectivity versus *iso*butane conversion for heteropoly acids or their salts (one or more of Cs^{+}, NH^{4+}, Ni^{2+} and Cu^{2+} as counter-cations) as catalysts based on reported literature.

Bifunctional catalysts with acidic and redox properties can activate the C-H bond [6–9], and redox properties have obviously a strong influence on the oxygen insertion reaction with lattice oxygen O^{2-}, which is known to lead to the formation of the desired products [10]. Of no exception, Keggin heteropolyacids (HPA), exhibiting Brønsted acidity and redox properties, have been extensively investigated for the selective oxidation of *iso*butane [11]. Although much effort has been made to design different efficient Keggin-type HPA catalysts using various cations such as Cs^{+}, NH_4^{+}, Ni^{2+} and Cu^{2+}, or/and loading them on different supports such as SiO_2 and $Cs_3PMo_{12}O_{40}$, the yield to MAA and MAC never exceeded 5% [2,12–19]. As one can see from **Fig. 1**, there is a barrier to high yield: when the conversion of *iso*butane increases, the selectivity to MAA and MAC decreases [20]. However, it should be noted that these results were always obtained in a fixed-bed reactor where the *iso*butane is fed together with oxygen or

air through a packed catalyst bed. As most catalytic oxidation reactions, the selective oxidation of IBAN to MAA and MAC proceeds *via* a Mars-Van Krevelen (MVK) mechanism, which was confirmed by Paul *et al.* [21] for HPA catalysts. In the MVK model, *iso*butane reacts with the lattice oxygen to form MAA and MAC before the reduced sites of the catalyst are re-oxidized by gas phase oxygen [22]. Correspondingly, the lattice oxygen from the catalyst plays an important role in the selective product formation. On the contrary, the interaction of *iso*butane with adsorbed oxygen from the gas phase is detrimental, and leads to the formation of CO_x and other degradation products such as acetic acid [23]. When reactant and oxygen are co-fed, these surface oxygen species will inevitably lead to non-selective oxidation.

Consequently, next to the design of new catalysts, the decoupling of the redox mechanism, meaning the separation of the reactant oxidation and the catalyst re-oxidation, seems highly promising to increase the yield. This method is successfully employed for the regenerating of catalysts deactivated by coke deposition, where the reaction is temporarily stopped and oxygen is injected for a period of time until the catalyst is regenerated and continues to operate [23–26]. This is often referred to as a semi-regenerative operation. In our case, this approach provides a well-defined temporal separation of the reduction and re-oxidation reactions.

Alternatively, to the temporal separation, a spatial separation of the reduction and re-oxidation will be studied using a two-zone fluidized bed reactor (TZFBR). The latter was already reported for the oxidative coupling of methane [27–31]. Comparable to a classical fluidized bed reactor, the employed TZFBR consists of a catalyst bed that is fluidized by a mixture of air and nitrogen but with an injection of IBAN in the middle of the bed (**Fig. 2.**). The intermediate injection of IBAN will separate the reactor into two zones: the zone above the injection point where only the oxidation of IBAN takes place (reaction zone) and the zone below the injection point where the reduced catalyst is re-oxidized by the oxygen from the fluidizing gas and consumes all oxygen (re-oxidation zone).

To the best of our knowledge, these concepts - a periodic reactor and a TZFBR - will be applied for the first time to the selective oxidation of *iso*butane to MAA and MAC over Cs-based Keggin type HPA catalysts.

2. Experimental section

2.1. Materials syntheses

The preparation of $H_4PMo_{11}VO_{40}$, has been described in previous work [32].

The CARiACT® SiO_2 - Q10, commercially available from Fuji Silysia Chemical Company, was used as a support. The SiO_2 has a specific surface area of 264 m^2/g, total pore volume of 1.12 cm^3/g, pore size of 17 nm, average particle diameter of 200 μm. The preparation of 40 wt.% $Cs_2H_2PMo_{11}VO_{40}$, supported on SiO_2 (in the following referred as $40CsV_1$) was carried out in two steps: *1)* SiO_2 was impregnated with Cs_2CO_3 (Fluka). *2)* The as-prepared support was then impregnated with $H_4PMo_{11}VO_{40}$. The detailed preparation is described in our previous work [32].

2.2. Characterization

X-ray diffraction patterns (XRD) were recorded in ambient conditions using the Cu Kα radiation (λ = 1.5418 Å; 40 kV, 30 mA) on a Siemens D5000 diffractometer, with a 0.02° scan step and 1 s time step in the 10-80° range. The interpretation of the diffractograms was performed using the Diffrac Eva software and by comparison by JCPDS reference files.

IR-Raman spectra were collected on a Horiba Xplora using a laser beam of 532 nm wavelength for excitation in confocal mode. A 50x long working distance objective (Olympus) was used for both focusing the excitation beam on the sample and collecting the scattered light. The latter was dispersed using an 1800 grooves spectrometer grating after having passed through a confocal hole of 300 μm. A Peltier-cooled CCD detector was used for recording the Raman spectra.

Surface analyses by X-ray Photoelectron Spectroscopy (XPS) were collected on an Axis Ultra DLD *"2009"* Kratos spectrometer using the monochromatic Al Kα radiation (hv = 1486.6 eV) as the excitation source. The calibration of the XPS spectra was made using the carbon C 1s reference peak at 284.8 eV. Simulation of the experimental photopeaks was carried out using Casa XPS software.

2.3. DFT Calculations

With respect to the complex mixture of the catalyst, the latter was simplified for computation using only the Keggin anion ($PMo_{11}VO_{40}^{4-}$). We performed spin-polarized DFT calculations using VASP software [33], with the Perdew-Burke-Ernzerhof (PBE) functional [34]. To avoid any interaction with periodic images, the Keggin structure was set in a 25x25x25 $Å^3$ box with fixed dimensions. All the calculations are performed at the gamma center, with a cutoff energy of 400 eV in the plane augmented wave (PAW) framework [35]. We chose an electronic convergence criterion of 10^{-6} eV, and an ionic convergence criterion of 0.05 eV/ Å. All those parameters allow to converge adsorption energies within ~0.05 eV.

2.4. Catalytic oxidation of *iso*butane in a periodic reactor

Selective oxidation of *iso*butane to MAC and MAA was carried out in semi-regenerative operation conditions. Thereby, the reactor was fed alternatively by IBAN and oxygen. In our case, catalytic reaction and catalyst regeneration were carried out with a fixed periodic cycling time [2,16]. The reactants, *iso*butane and O_2 were diluted with inert argon and helium as an internal standard. The principle of the alternating flows consists of having three gas flows: *(i)* central Ar flow is fed continuously whereas *(ii)* two lateral Ar serve for replacing the reactant (He-IBAN) or oxidant (He-O_2) gases. The flow-rates of each gas are regulated by mass flow controllers (MFC - BROOKS). Water was introduced *via* the central argon gas line by means of a saturation system, keeping 10 % partial pressure of water in the overall gas stream calculated according to the Antoine equation. A schematic diagram of the system is shown in **Fig. S1**.

The mixture fed during periodic operation remains at a constant total flow-rate of 44.5 mL/min STP. The molar ratios were 56.2 % Ar, 10.1 % H_2O, 15.7 % IBAN and 18.0 % He (or 22.5 % O_2 and 11.2 % He), corresponding to a contact time of 3 s (*approx.* WHSV is 1.8 $L \cdot g^{-1} \cdot h^{-1}$). During a typical periodic feed cycle, the reductant gas (Ar-H_2O-He-IBAN) passes through the reactor for 2 min. Afterwards, to remove this gas from the reactor, inert gas (Ar-H_2O) passes through the system for 1 min. Next, oxidant gas (Ar-H_2O-He-O_2) flows through

the system for 3 min to oxidize the solid. To remove unreacted or excess oxygen from the system, again, Ar-H_2O gas flows through the reactor for another 1 min.

The catalytic reaction was carried out under 1 atmosphere. The temperature explored was 340 °C. Typically 1.5 g of catalyst solid were employed. All products were analyzed by online mass spectrometer (Balzers Prisma, QMS200). The mass spectrometer (MS) continuously samples from the outlet of the reactor. At the beginning and end of each test, the Ar, He, IBAN and O_2 sensitivities were calculated using a by-pass periodic feed sequence. The response factors for all products were obtained by calibration of the MS during a classical fixed bed catalytic test [32]. The mass spectrometer background signals were also determined during this sequence. Quantitative information was obtained by integrating the reactant or product during a full cycle.

2.5. Catalytic oxidation of *iso*butane in a two-zone-fluidized bed reactor (TZFBR)

The TZFBR is schematically shown in **Fig. 2**. Oxidizing gas (air) enters along with fluidization gas (nitrogen) from the bottom of the reactor into the system. The reactant gas (*iso*butane) and carrier gas (helium) saturated with water vapor, are injected through the nozzle in the center of the fluidized bed. The reaction conditions were as follows: The reactants mixture was fed at a constant total flow-rate of 20 mL/min STP (molar ratio 35 % IBAN; 10 % H_2O; 55 % He). The fluidized gas is controlled by a rotameter (Q-Flow-Vögtlin) and the flow rate of 70 L/h STP corresponding to 2 times the minimum fluidization velocity (the hydrodynamic of the TZFBR are described in ESI). The oxidant gas was fed at the flow rate with molar ratio O_2 to IBAN of 0.6, 2, 3, and 6 depending on the catalytic test. The catalytic experiments were performed using 20 g of catalyst (40 wt.% of $Cs_2H_2PMo_{11}O_{40}$ on SiO_2) diluted in 80 g of SiO_2. The mechanical stability of the catalyst was evaluated before (*cf. ESI* for detailed information). Before the test, the reactor was heated to reaction temperature (340 °C), and the reactant gas was injected *via* the inlet tube when the temperature was reached. The products and non-reacted IBAN were analyzed by gas-chromatography and cold traps, as described in [32].

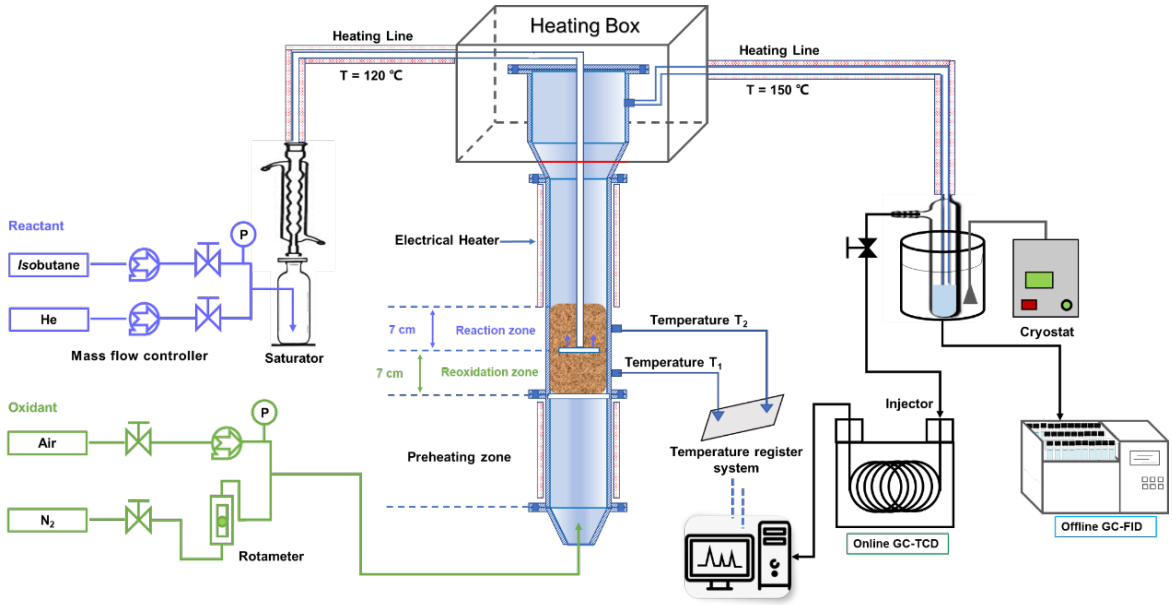

Fig. 2. Schematics of the TZFBR set-up.

3. Results and discussion

3.1. Catalytic evaluation in *iso*butane oxidation reaction in periodic conditions

First, the catalytic performance of $40CsV_1$ was evaluated with a reduction step of a 2 min for the reaction and 3 min for the re-oxidation cycle (2R-3O) at 340 °C to understand its instantaneous performance. In **Fig. 3**, the instantaneous conversion of *iso*butane and formed products are shown during the reaction cycle. As one can see, the *iso*butane conversion gradually decreased after 20 s as the available oxygen (lattice or surface oxygen) in the oxygen carrier ($40CsV_1$) is consumed. This decrease in conversion is accompanied by a decrease in CO and CO_2 formation in the first 20 s. Methacrolein is formed at the beginning of the reaction, before it gradually decreases. However, in the first 40 s of the reaction, the formation of methacrylic acid increased whereas the conversion of *iso*butane and the intermediate MAC decreased. After 40 s, the amount of MAC and MAA decreased since the available lattice oxygen is entirely consumed. Acetone and acetaldehyde are formed steadily during the reaction cycle, while the formation of acetic acid is coupled to the conversion of *iso*butane. The fact that acetone and acetaldehyde are constantly formed throughout the cycle suggests that both are products from the decomposition of MAC and MAA.

As seen before, the *iso*butane and oxygen signals changed during a cycle, meaning that the catalyst is never in a stationary regime. Correspondingly, the length of the cycling time is of significant parameter in a periodic reactor, whereby it was studied in more detail.

In the previous test, the cycling time was 2 min of *iso*butane and 3 min of oxygen (2R-3O) and the corresponding theoretical molar ratio of oxygen/*iso*butane was 2.14. In the following tests, the influence of the cycle time was studied by shortening the oxidation time, thus decreasing the oxygen/*iso*butane ratio. As shown in **Table 1**, when the reduction time was maintained at 2 min and the injection of O_2 was varied from 3 min to 0.2 min (theoretical molar ratio of oxygen/*iso*butane ranging from 2.14 to 0.14), the conversion of oxygen increased dramatically, while the conversion of *iso*butane decreased. The quantities of moles of O_2 and IBAN consumed are shown in **Table S1.**

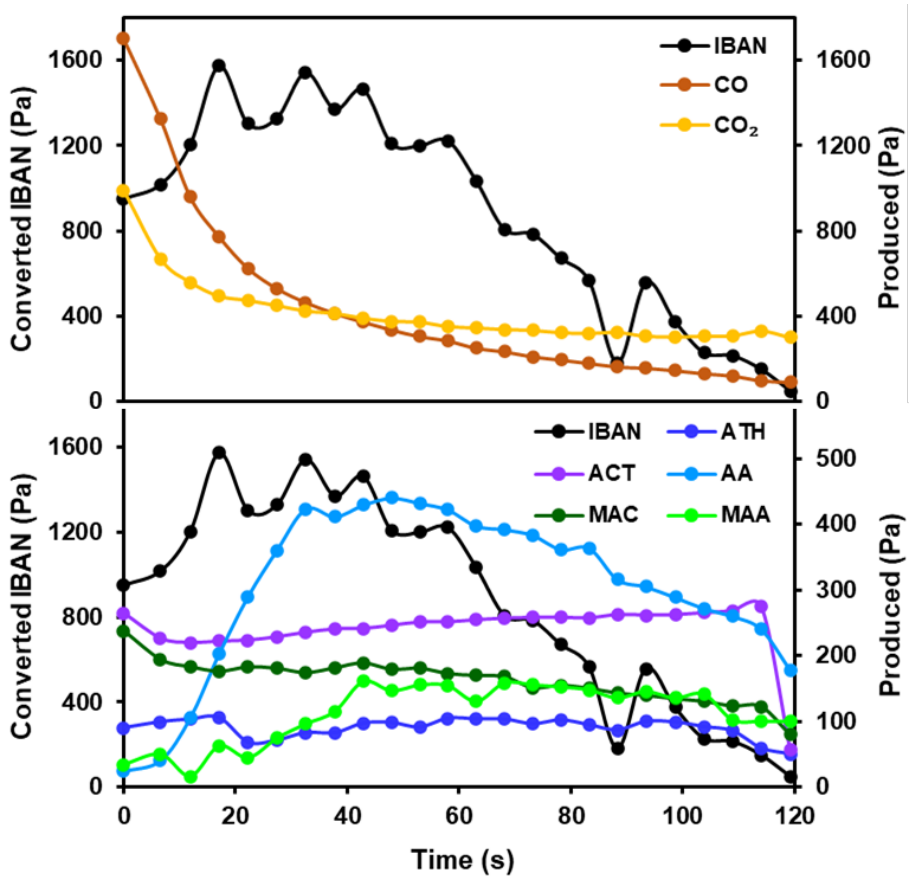

Fig. 3. Concentration profiles evolution during the reduction step (2 min) over $40CsV_1$ at 340 °C with a cycling time 2R-3O (IBAN = *iso*butane, MAA = methacrylic acid, MAC = methacrolein, AA = acetic acid, ACT = acetone and ATH = acetaldehyde).

Table 1.

Catalytic performance in IBAN oxidation of 40CsV_1 sample with different cycling times.

Molar ratio O_2/IBAN	Cycling time	Conversion [a], %		Selectivity, %							Carbon balance, %
		O_2	IBAN	MAA	MAC	CO	CO_2	ATH	ACT	AA	
2.14	2R-3O	4.0	5.8	12.1	18.5	13.1	11.4	5.9	20.5	17.2	99.9
1.43	2R-2O	5.8	5.7	13.7	18.2	11.1	12.0	6.4	22.9	14.5	99.6
0.71	2R-1O	8.8	4.7	13.7	21.7	6.1	12.6	5.6	29.1	10.0	99.7
0.36	2R-0.5O	15.3	4.3	20.3	22.4	5.5	10.9	4.2	25.9	9.5	99.9
0.14	2R-0.2O	30.8	3.2	11.8	22.3	6.9	13.1	5.5	30.8	7.8	99.4

[a] Reaction conditions: Atmospheric pressure, Contact time: 3 s; Reaction temperature: 340 °C; IBAN = *iso*butane, MAA = methacrylic acid, MAC = methacrolein, AA = acetic acid, ACT = acetone and ATH = acetaldehyde.

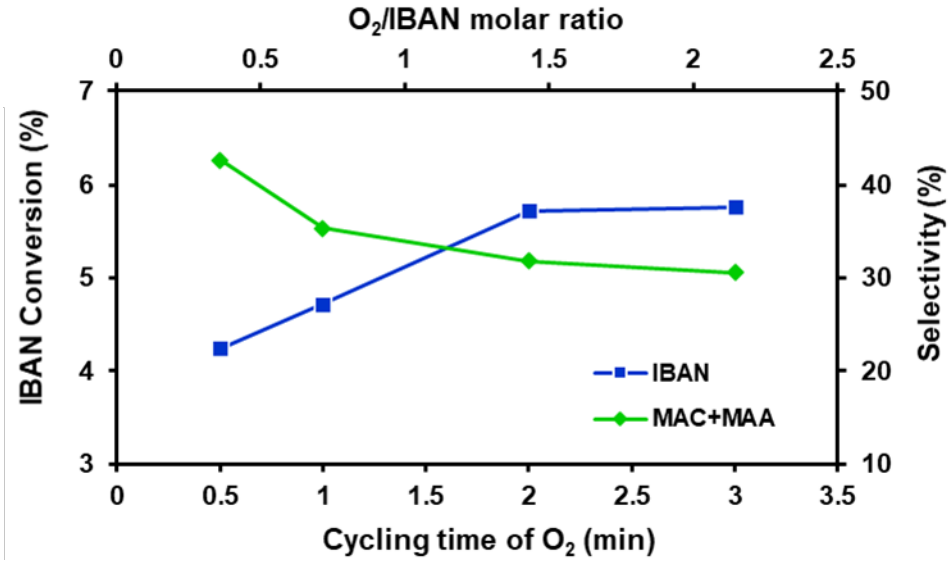

Fig. 4. IBAN conversion and MAA+MAC selectivity on 40CsV_1 sample at 340 °C with a cycling time of 2 min for the reduction and from 3 to 0.5 min for reoxidation.

However, when the cycling time of O_2 increased from 0.5 to 3 min, the conversion of IBAN and the selectivity to the main products (MAA and MAC) changed and reached a plateau at 2 min (O_2/IBAN = 1.43), as can be observed in **Fig. 4**. The presence of this plateau indicates that even at oxygen/*iso*butane ratio of 1.43, the oxygen injected during the reoxidation cycle was still not the limiting factor. This is in good agreement with the XPS results (*cf.* 3.3.2), showing that the ratio of V^{5+}/V^{4+} in spent catalyst was increased compared to the fresh catalyst, meaning that more V^{4+} was oxidized by the excess of oxygen. Furthermore, the selectivity to the main products increases with decreasing the oxygen cycle time and reached a maximum

(42.7 %) for a molar ratio of O_2/IBAN of 0.36. At the same time, the selectivity to CO_x decreased to its minimum (16.4 %).

More detailed information about the impact of the sampling time is shown in **Fig. 5**. It can be clearly observed that the *iso*butane conversion decreased more rapidly during a cycle when the reoxidation time was shorter and therefore the O_2/IBAN ratio smaller (**Fig. 5A**). The selectivities to the main products MAA and MAC are also shown in **Fig. 5B**. In a single cycle, the amount of produced MAA and MAC increases during the first 40 s, and then logically decreases as the available oxygen in the oxygen carrier ($40CsV_1$) is consumed.

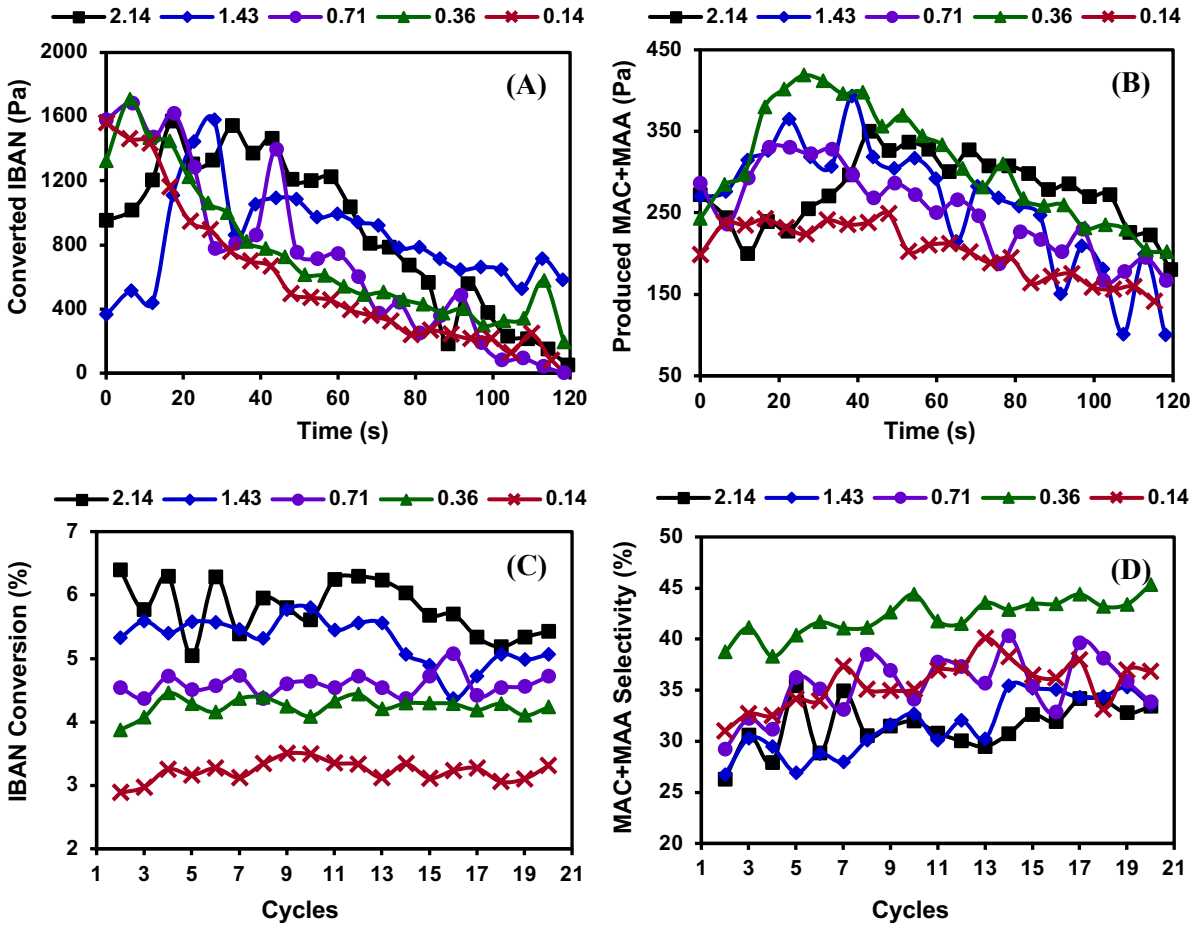

Fig. 5. Conversion and selectivity on $40CsV_1$ sample with different molar ratios of O_2/IBAN at the reaction temperature of 340 °C. The molar ratios of O_2/IBAN were: 2.14, 1.43, 0.71, 0.36 and 0.14. (A) and (B) show the reduction part of a cycle, while (C) and (D) show the changes during the periodic tests.

For the comparison of all the cycles of an experiment (**Fig. 5C**) one can see that the use of higher quantities of oxygen was favorable for the IBAN conversion. With an O_2/IBAN molar

ratio of 2.14, a mean conversion of 5.8 % was observed during the periodic test. On the other hand, high O_2/IBAN molar ratio led to a decrease in MAA and MAC selectivity (**Fig. 5D**). This decrease in MAA and MAC selectivity can be explained by the decomposition of the as-formed products due to the excess of oxygen [24]. One can further conclude from **Fig. 5C** and **D** that the catalyst maintains a good oxygen uptake- and release-capacity throughout the 20 reaction cycles, thus conserving a stable performance. Moreover, the catalyst was not constantly over-reduced according to the XPS of the spent catalysts (**Table 3**), irrespective of the conditions. It is noteworthy that there are two other phenomena that can be seen from **Fig. 5D**: First, the selectivity to the desired products seems to increase in the initial few cycles (≤ 10 cycles), and then tends to stabilize, especially when the molar ratio of O_2/IBAN is less than 0.71. This might be explained by the large specific surface area of the catalyst and its pore structure, where oxygen species will be present on the catalyst surface as physisorbed species – despite the intermediate flushing with inert gas. Thus, only after the physisorbed oxygen species are consumed, the selectivity to the desired products increases. Another phenomenon is that when the O_2/IBAN molar ratio is further reduced from 0.36 to 0.14, the decrease in *iso*butane conversion is accompanied by a slight decrease in the selectivity to MAA and MAC. The latter can be explained by the fact that the short oxygen cycling time was not sufficient to completely re-oxidize the catalyst or that oxygen species were not able to completely enter the bulk of the catalyst to form lattice oxygen during the regeneration step. The non-entirely regenerated catalyst cannot promote the reaction causing the decrease of the *iso*butane conversion. All in all, the reaction is more favorable when the molar ratio of O_2/IBAN is 0.36.

The catalytic performance of the same catalyst was also evaluated under co-feed conditions at the same temperature as shown in **Fig. 6** (the molar ratio O_2/IBAN was 0.43). The selectivity to MAC and MAA was 25 % with 33.6% selectivity to CO_x (10.2 % *iso*butane conversion). Of course, the periodic reaction separates the reduction from the oxidation process and reduces the conversion of *iso*butane, thus also reducing the formation of products from over-oxidation.

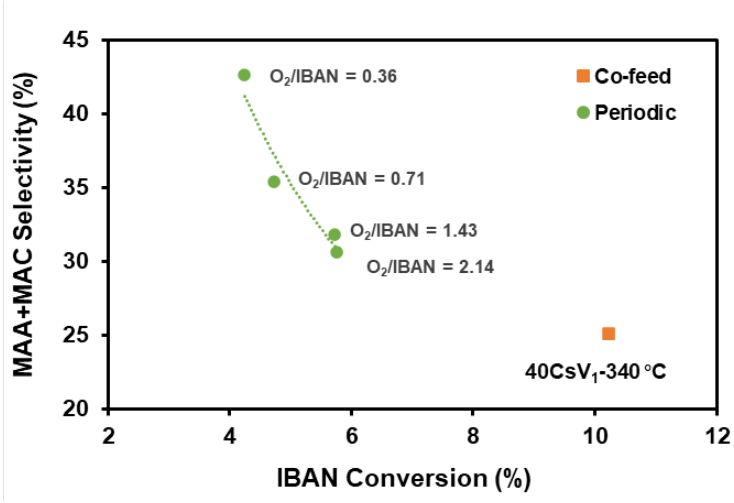

Fig. 6. Relationship between IBAN conversion and selectivity to (MAC+MAA) obtained on $40CsV_1$ catalyst under periodic and co-feed conditions at 340 ºC.

3.2 Catalytic performance evaluation in the TZFBR

A two-zone fluidized-bed reactor was employed for the selective oxidation of *iso*butane to methacrylic acid and methacrolein. In optimal conditions, all the oxygen present in the fluidization gas is consumed by the reoxidation of the catalyst in the zone below the IBAN injection nozzle. Therefore, the effect of the O_2/IBAN molar ratio was studied varying the oxygen concentration in the fluidizing gas. The molar ratios of O_2/IBAN were 6, 3, 2 and 0.6 respectively. It's worth mentioning that the molar ratio of 2 is the theoretical molar ratio for the selective oxidation of *iso*butane to methacrylic acid. As one can see from the results (**Table 2** and **Fig. 7**), the conversion of IBAN significantly increased with the O_2/IBAN ratio, reaching 15.4% for a ratio of 6. This increase of IBAN conversion was accompanied by the decrease of the oxygen conversion which was only 10.9 % for the same O_2/IBAN ratio (6) but 18.6% for a ratio of 0.6. However, no matter the reactions conditions, the main products observed were CO_x and C2 compounds, which indicates that MAC and MAA are probably decomposed in the TZFBR. This significant decomposition could be explained by i) the large volume of the disengagement leading to a high contact time of all products in the heated zones or ii) the low IBAN conversion. In fact, since the IBAN conversion was <15%, oxygen was not entirely consumed in the reoxidation zone (the oxygen conversion was never above 20 %). Correspondingly, this excess of oxygen reached the reaction zone and could lead to degradation

of MAC and MAA to CO_x. According to kinetic studies, the rate constants for desired products decomposition are 50 times higher than that for MAA and MAC formation [21]. Due to these technical limitations, it was not possible to conclude on the viability of the TZFBR concept for the selective oxidation of IBAN.

Table 2

Catalytic performance in IBAN oxidation for $40CsV_1$ with different oxygen/*iso*butane molar ratios.

O_2/IBAN molar ratio	Conversion [a], %		Selectivity, %				Carbon balance, %
	O_2	IBAN	CO_x	AA	ACT	Others	
6	10.9	15.4	92.3	2.5	-	5.2	98.9
3	16.9	13.4	90.2	1.8	-	8.0	98.7
2	19.1	10.5	87.9	2.2	-	9.9	98.8
0.6	18.6	3.3	75.4	6.6	1.8	16.2	98.2

[a] Reaction conditions: Temperature = 340 °C, atmospheric pressure, contact time 6.8 s.
IBAN = *iso*butane, AA = acetic acid and ACT = acetone.

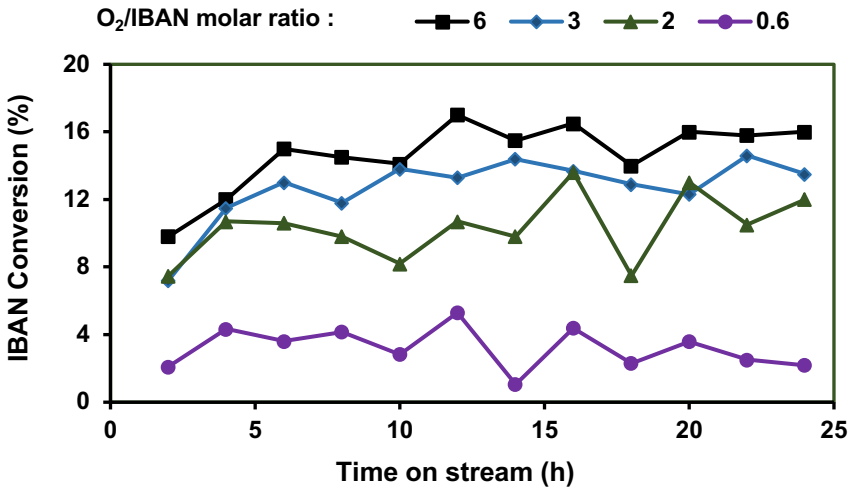

Fig. 7. Influence of the O_2/IBAN molar ratio on the IBAN conversion (*T.* = 340 ºC).

3.3. Physicochemical properties of the catalysts

3.3.1. Crystal phases and structural features analysis by XRD and Raman

The physical and structural properties of fresh and spent catalysts following the catalytic tests in a periodic reactor under atmospheric pressure were determined. The XRD patterns of the fresh and spent $40CsV_1$ catalysts are shown in **Fig. 8A**. All diffractograms are similar before and after reaction, implying that there is no significant alteration of the Keggin structure during

the test under periodic conditions. This further indicates that the active phase impregnated on the SiO_2 support exhibits excellent thermal stability. It should also be noted that the diffraction peaks of the spent catalyst become narrower compared to those of the fresh one, implying an increase in crystallinity of the catalyst after reaction, probably due to sintering [32]. The Raman spectra of supported $40CsV_1$ catalyst is shown in **Fig. 8B**. The existence of the Keggin structure is characterized by the presence of the following well-known vibration bands [36,37]: ν_s (Mo=O_d) at 983 cm^{-1}, ν_{as} (Mo-O_b-Mo) at 871 cm^{-1}, ν_{as} (Mo-O_c-Mo) at 600 cm^{-1} and δ (Mo-O-Mo) at 255 and 235 cm^{-1}, respectively. The absence of vibration bands at 818 cm^{-1} and 660 cm^{-1}, which can be attributed to crystalline MoO_3, further confirms that the active phase is well stabilized on the support [38].

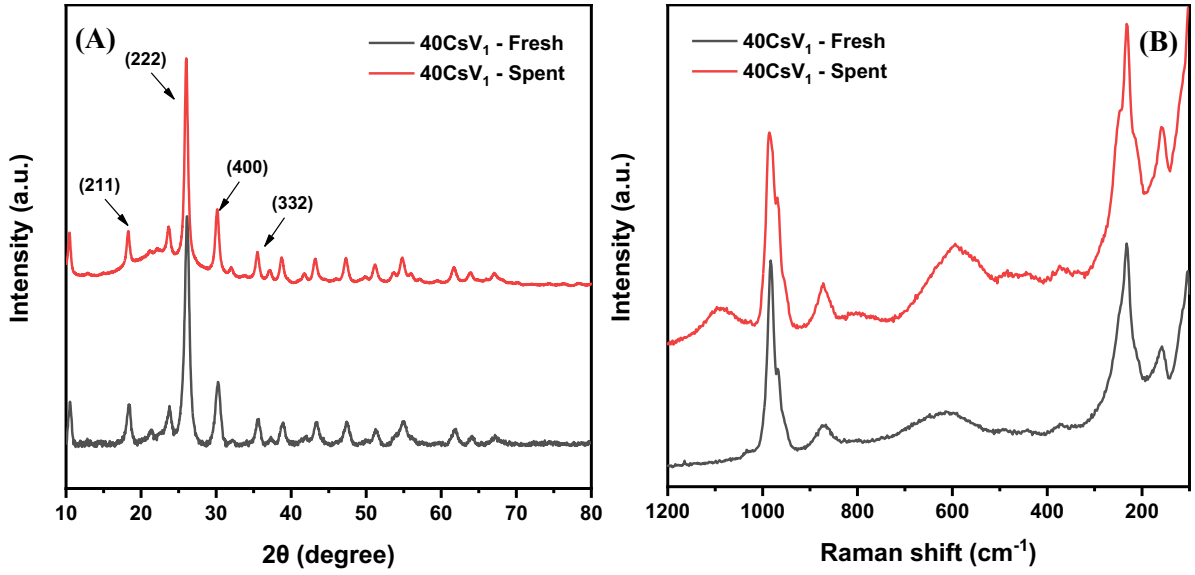

Fig. 8. XRD patterns (A) and Raman spectra (B) of the fresh and spent $40CsV_1$ catalysts. The spent catalyst was tested at a cycling time of 2R-3O.

3.3.2. Surface analysis by XPS

X-ray photoemission spectroscopy measurements were carried out on the fresh and spent CsV_1/SiO_2 samples in periodic reactor to investigate the oxidation states of the vanadium and molybdenum and to estimate the surface compositions. All spectra were analyzed by a peak-fitting procedure. The peaks assigned to vanadium ($V2p_{3/2}$) and molybdenum ($Mo3d_{5/2}$, $Mo3d_{3/2}$) are reported in **Fig. 9**. The BE values of the $V2p_{3/2}$, $Mo3d_{5/2}$ and $Mo3d_{3/2}$ are gathered

in **Table 3**. The peak of $V2p_{3/2}$ was deconvoluted to V^{5+} and V^{4+} at 518 and 517 eV [36,39], the peaks $Mo3d_{5/2}$ and $Mo3d_{3/2}$ were deconvoluted to Mo^{6+} and Mo^{5+} at 232.7/231.4 eV and 235.8/234.5 eV [40,41], respectively. The V^{5+}/V^{4+} and Mo^{6+}/Mo^{5+} ratios were calculated according to the area of the corresponding peaks.

From the results one can see that the V^{5+}/V^{4+} (or Mo^{6+}/Mo^{5+}) ratio for the spent catalyst increased slightly compared to the fresh one (the cycling time of 2R-3O and 2R-2O), as shown in **Fig. 9** and **Table 3**Erreur ! Référence non valide pour un signet.. It can be assumed that this change is caused by the oxidation of the catalyst during the cyclic test. It should be noted that all periodic tests started with the reduction of the catalyst (*i.e.,* the catalytic reaction) and ended with the reoxidation of the catalyst. In the fresh sample, V^{4+} was dominating, but a mixture of V^{4+} and V^{5+} was observed, indicating that there was not enough oxygen to react with the vanadium atoms during the synthesis process, which might result from the drying of the samples under vacuum conditions after the impregnation. The reduction of the transition metal centers (V, Mo) may be explained by the oxidation of O^{2-} ligands (lattice oxygen) to molecular O_2, which is lost to the environment (also called autoreduction) [42]. During the catalytic reaction, the catalyst was re-oxidized at reaction temperature and in the presence of oxygen.

In addition, the influence of reduction time and re-oxidation time employed in the periodic reactor on the oxidation state of vanadium and molybdenum was studied. The amount of oxygen injected in the cycling test for the $40CsV_1$ sample at 340 °C gradually decreased with each cycle as the oxidation time varied. As one can see, the V^{5+}/V^{4+} ratio decreased with decreasing O_2/IBAN ratio, from 42/58 for an oxygen/IBAN ratio of 2.14, to 31/69 for an oxygen/IBAN ratio of 0.14. This can be explained by the redox mechanism of the reaction: vanadium V^{5+} is consumed when *iso*butane is oxidized (reaction step) and re-oxidized to V^{5+} in the reoxidation step. Correspondingly, an increased re-oxidation cycle allows to re-oxidize more V^{4+} to V^{5+} whereby the V^{5+}/V^{4+} increases. Simultaneously, the Mo^{6+}/Mo^{5+} ratio has similar tendency. However, the observed performance in **Table 1** showed that when the oxygen injection time is too long, more highly oxidized products are formed, which also indicates the presence of unselective forms of adsorbed oxygen species on the surface.

Table 3.

Surface analysis results for the 40CsV$_1$ samples before and after reaction

Catalysts	Cycling time	Molar ratio O_2/IBAN	Binding energy (BE), eV	V^{5+}/V^{4+} ratio	Binding energy (BE), eV		Mo^{6+}/Mo^{5+} ratio
			$V2p_{3/2}$, V^{5+}/V^{4+}		$Mo3d_{5/2}$, Mo^{6+}/Mo^{5+}	$Mo3d_{3/2}$, Mo^{6+}/Mo^{5+}	
Fresh	-	-	518.0/516.9	35 / 65	232.6/231.4	235.8/234.5	88.9 / 11.1
Spent [a]	2R-3O	2.14	518.1/516.8	42 / 58	232.6/231.4	235.8/234.5	100 / 0
	2R-2O	1.43	518.1/516.9	39 / 61	232.6/231.4	235.7/234.5	89.2 / 10.8
	2R-1O	0.71	518.1/516.8	34 / 66	232.6/231.4	235.7/234.5	88.5 / 11.5
	2R-0.5O	0.36	518.1/516.9	32 / 68	232.7/231.4	235.8/234.5	88.0 / 12.0
	2R-0.2O	0.14	518.1/516.9	31 / 69	232.7/231.4	235.8/234.5	86.4 / 13.6

[a] Reaction temperature: 340 ºC.

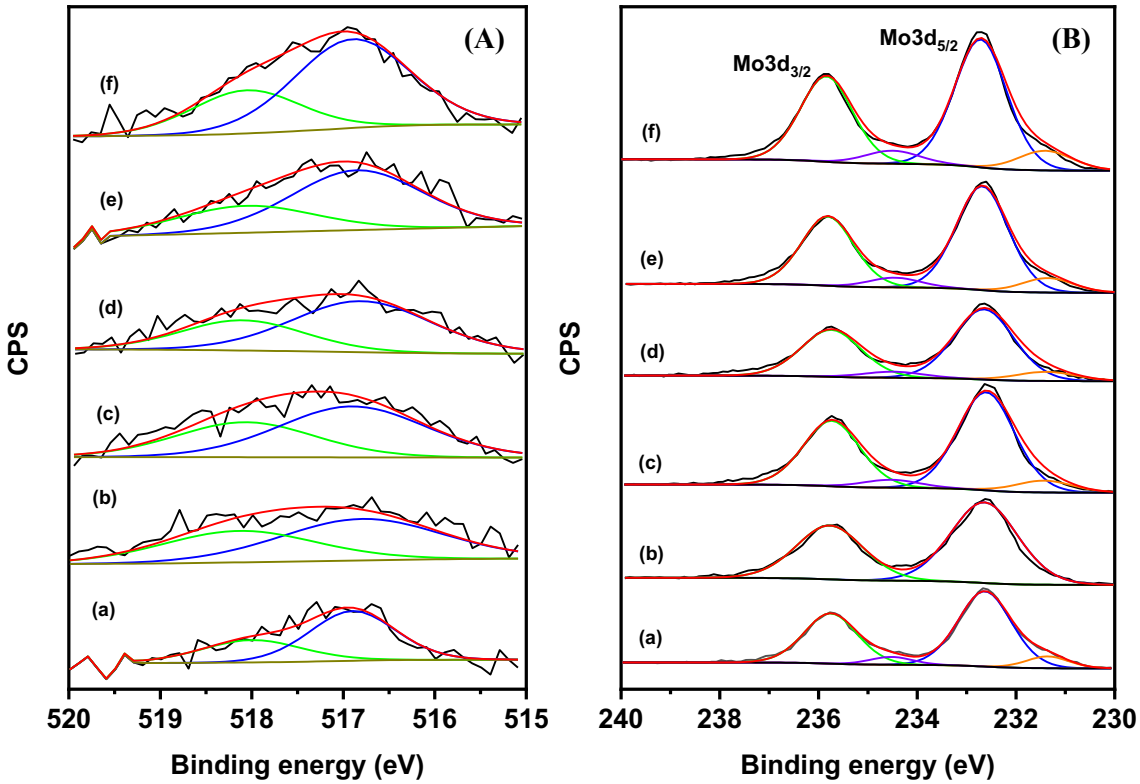

Fig. 9. XPS spectrum of (A) V2p and (B) the Mo3d for the 40CsV$_1$ samples: Fresh catalyst (a) and spent catalysts at 340 °C with different O_2/IBAN molar ratios: (b) 2.14, (c) 1.43, (d) 0.71, (e) 0.36, (f) 0.14.

The catalyst employed in the TZFBR was also analyzed by XPS. **Fig. 10** presents the peaks of vanadium ($V2_{P3/2}$) in the fresh and spent catalysts. The BE values of vanadium ($V2_{P3/2}$) are collected in **Table 4**. As can be seen from the results, the V^{5+}/V^{4+} ratio and the Mo^{6+}/Mo^{5+} ratio of the spent catalyst increased from 35/65 to 42/58 and 88.9/11.1 to 95.2/4.8, respectively,

compared to the fresh catalyst. This phenomenon was also caused by the regeneration of the catalyst by oxygen during the fluidization test.

Table 4.

Surface analysis results for the samples before and after reaction used in the TZFBR

Catalysts		Binding energy (BE), eV	V^{5+}/V^{4+} ratio	Binding energy (BE), eV		Mo^{6+}/Mo^{5+} ratio
		$V2p_{3/2}$, V^{5+}/V^{4+}		$Mo3d_{5/2}$, Mo^{6+}/Mo^{5+}	$Mo3d_{3/2}$, Mo^{6+}/Mo^{5+}	
$40CsV_1$	Fresh	518.0/516.9	35 / 65	232.6/231.4	235.8/234.5	88.9 / 11.1
	Spent [a]	518.0/516.9	42 / 58	232.7/231.4	235.8/234.5	95.2 / 4.8

[a] Reaction temperature: 340 ºC.

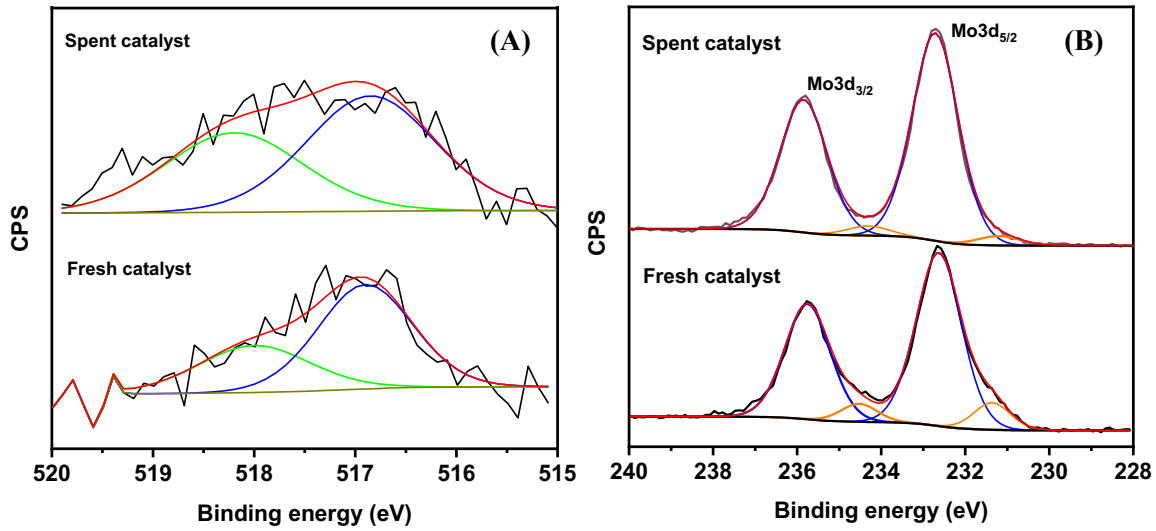

Fig. 10. XPS spectrum of (A) V2p and (B) the Mo3d for the $40CsV_1$ samples before and after reaction in TZFBR.

4. DFT Calculations

With respect to the observed poor catalytic performance, DFT calculations were performed in order to confirm the hypothesis of a competing mechanism between the formation of MAA/MAC and CO_2. We considered the HPA catalyst without any O vacancy as the starting point of any catalytic cycle. For each reaction intermediate, we considered various adsorption sites, either at a metal atop O, or at a metal-metal bridging O. Also, O atoms can be linked either with Mo or with V metals, hence leading to four non-equivalent adsorption sites: Mo or V atop O, and Mo-Mo or Mo-V bridging O. According to our calculations, the V atop O position is always the most stable, and it will be used for every adsorbate in the following. The global reaction pathways are represented in **Fig. 11**, and the structures in **Fig. S7**.

Once IBAN adsorbs at the HPA, it can follow two different pathways, either toward MAC/MAA in red (cd. **Fig. 11**), or in to CO_2 in orange (cf. **Fig. 11**). The first path, in red, includes three successive catalytic cycles (see **Fig. 11**). The first one, implying exothermic C-C breaking in IBAN is very favorable on the thermodynamic point of view and leads to *Iso*butene formation. Then, *Iso*butene is oxidized into MAC in a slightly exothermic surface process. And finally, at the last catalytic cycle MAC is oxidized into MAA in a highly exothermic step. Regarding the second potential reaction pathway in orange, it also consists in three catalytic cycles (see **Fig. S7**). It starts with the IBAN athermic decomposition at the HPA into methanol (MeOH) and acetone. Then, acetone is oxidized into acetic acid (MeCOOH) and formaldehyde (CH_2O). This step is exothermic at the catalyst surface. And finally, in a highly exothermic process formaldehyde is oxidized into carbon dioxide (CO_2).

As a result, both pathways mainly present exothermic surface steps at HPA catalyst, giving rise to a competition between the two products. However, regarding the global process presented in **Fig. 11**, CO_2 formation (-11.00 eV) from IBAN is more exothermic than MAA production (-10.64 eV). This difference is enough to explain that CO_2 formation is an inevitable side reaction in IBAN oxidation process.

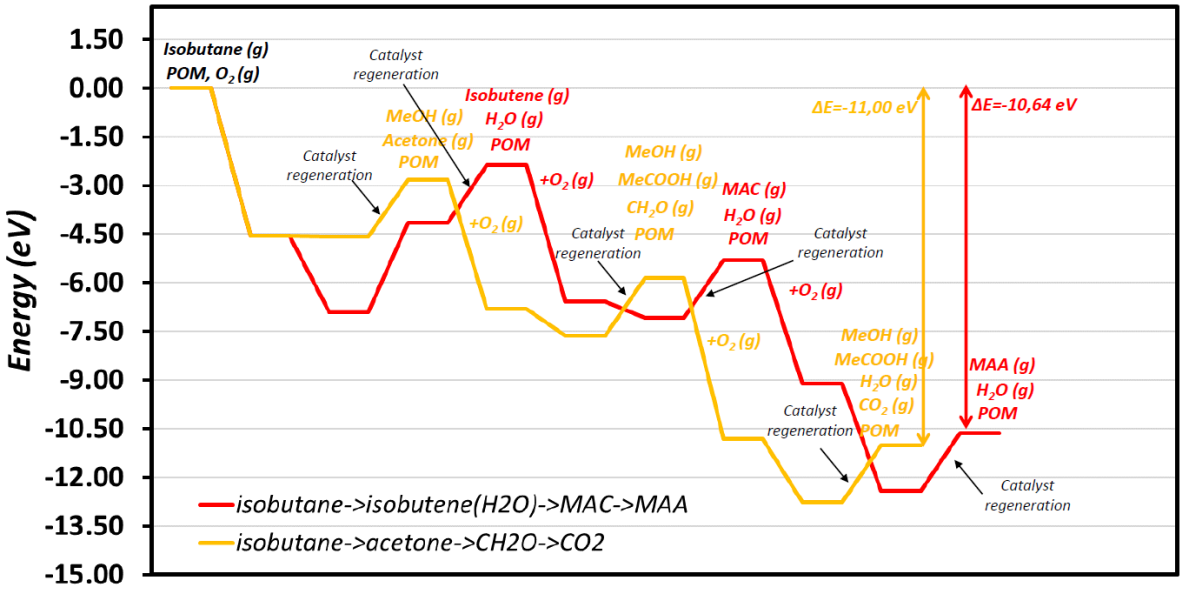

Fig. 11. Energy barriers for the selective oxidation of IBAN to MAC/MAA (red) and the non-selective oxidation to CO_2 (yellow). POM=Polyoxometalate.

5. Conclusions

The redox decoupling concept using periodic reactor and the TZFBR was applied for the first time to the selective oxidation of *iso*butane to methacrolein and methacrylic acid using a HPA-based catalyst. In contrast to co-feed conditions in a classical fixed-bed reactor, the reactant and oxidant are separated by a time gap under periodic conditions and spatially in the TZFBR. The periodic reactor tests notably allow to obtain precise information about the product formation during the *iso*butane reaction step. Thereby, the effect of the cycling time between reaction and reoxidation step (and hence of the molar ratio of oxygen/*iso*butane injected in each cycle) were studied. It was found that increasing the O_2/IBAN ratio resulted in increased conversion, but to the expense of the selectivity to MAA and MAC. $40CsV_1$ catalyst presented the highest MAC+MAA selectivity of 42.7 % (4.3 % IBAN conversion) with the molar ratio of O_2/IBAN = 0.36 at 340 ºC reaction temperature. Furthermore, the presence of adsorbed unselective oxygen species could not be excluded even by the intermediate flushing of the catalyst by inert gas. These species led to large amount of CO_x formation in the beginning of the reaction cycle. On the other hand, the formation of MAC and MAA increased in the beginning of the reaction cycle and passed through a maximum, confirming that the selective oxidation is based on lattice oxygen species and the CO_x is not yielding from the decomposition of MAC and MAA, but from the direct oxidation of IBAN.

The catalysts before and after the reaction in the periodic reaction were characterized showing that they exhibited a high stability during the periodic reaction process, as can be seen from XRD and Raman. The crystal structure of the catalyst did not decompose, and the active phase was still present after test. The presence of V^{4+}/V^{5+} species in the catalysts before and after the reaction indicates that vanadium was constantly reduced and re-oxidized under reaction conditions (Mars-Van Krevelen mechanism), underlining the good redox properties of the catalyst.

Using the TZFBR, however, yielded only non-selective catalytic oxidation. Even the change of the oxygen concentration in the fluidization gas did not allow to obtain the desired products. The possible reasons may be the decomposition of MAC and MAA in the huge dead

volume of the reactor (disengagement section) or the presence of non-reacted oxygen in the reaction zone due to the low conversion of *iso*butane (usually less than 10 %).

Acknowledgements

This work has benefited from the support of the CSC-Groupe des Ecole Centrale PhD scholarship program (China-France). Chevreul Institute (FR 2638), Centrale Lille Institute, Ministère de l'Enseignement Supérieur, de la Recherche et de l'Innovation, Hauts-de-France Région and FEDER are acknowledged.

References

[1] F. Jing, B. Katryniok, E. Bordes-Richard, S. Paul, Catal. Today 203 (2013) 32–39.

[2] F. Jing, B. Katryniok, F. Dumeignil, E. Bordes-Richard, S. Paul, Catal. Sci. Technol. 4 (2014) 2938–2945.

[3] S. Liu, L. Chen, G. Wang, J. Liu, Y. Gao, C. Li, H. Shan, J. Energy Chem. 25 (2016) 85–92.

[4] M.J. Darabi Mahboub, J.L. Dubois, F. Cavani, M. Rostamizadeh, G.S. Patience, Chem. Soc. Rev. 47 (2018) 7703–7738.

[5] J. He, Y. Liu, W. Chu, W. Yang, Appl. Catal. A Gen. 556 (2018) 104–112.

[6] E. Bordes-Richard, Catal. Today (2019) 1–12.

[7] M. Misono, Chem. Commun. 1 (2001) 1141–1153.

[8] N. Mizuno, M. Misono, Chem. Rev. 98 (1998) 199–217.

[9] D. Vanhove, Appl. Catal. A Gen. 138 (1996) 215–234.

[10] L. Zhang, S. Paul, F. Dumeignil, B. Katryniok, Catalysts 11 (2021) 769.

[11] F. Jing, B. Katryniok, E. Bordes-Richard, F. Dumeignil, S. Paul, Catalysts 5 (2015) 460–477.

[12] Y. Liu, J. He, W. Chu, W. Yang, Catal. Sci. Technol. 8 (2018) 5774–5781.

[13] M. Langpape, J.M.M. Millet, U.S. Ozkan, M. Boudeulle, J. Catal. 181 (1999) 80–90.

[14] F. Cavani, R. Mezzogori, A. Pigamo, F. Trifirò, Chem. Eng. J. 82 (2001) 33–42.

[15] F. Cavani, R. Mezzogori, A. Pigamo, F. Trifirò, E. Etienne, Catal. Today 71 (2001) 97–110.

[16] N. Mizuno, H. Yahiro, J. Phys. Chem. B 102 (1998) 437–443.

[17] E. Etienne, F. Cavani, R. Mezzogori, F. Trifirò, G. Calestani, L. Gengembre, M. Guelton, Appl. Catal. A Gen. 256 (2003) 275–290.

[18] F. Cavani, R. Mezzogori, A. Pigamo, F. Trifirò, Top. Catal. 23 (2003) 119–124.

[19] M. Langpape, J.M.M. Millet, Appl. Catal. A Gen. 200 (2000) 89–101.

[20] M. Sultan, S. Paul, M. Fournier, D. Vanhove, Appl. Catal. A Gen. 259 (2004) 141–152.

[21] S. Paul, V. Le Courtois, D. Vanhove, Ind. Eng. Chem. Res. 36 (1997) 3391–3399.

[22] G. Mazloom, S.M. Alavi, React. Kinet. Mech. Catal. 110 (2013) 387–403.

[23] G. Mazloom, S.M. Alavi, Part. Sci. Technol. 36 (2018) 61–71.

[24] B. Katryniok, R. Meléndez, V. Bellière-Baca, P. Rey, F. Dumeignil, N. Fatah, S. Paul, Front. Chem. 7 (2019) 127.

[25] N. Song, C. Rhodes, J.K. Bartley, S.H. Taylor, D. Chadwick, G.J. Hutchings, J. Catal. 236 (2005) 282–291.

[26] G. Emig, K. Uihlein, C.J. Häcker, Stud. Surf. Sci. Catal. 82 (1994) 243–251.

[27] M.L. Pacheco, J. Soler, A. Dejoz, J.M. López Nieto, J. Herguido, M. Menéndez, J. Santamaría, Catal. Today 61 (2000) 101–107.

[28] R. Ramos, J. Herguido, M. Menéndez, J. Santamaría, J. Catal. 163 (1996) 218–221.

[29] J. Rischard, C. Antinori, L. Maier, O. Deutschmann, Appl. Catal. A Gen. 511 (2016) 23–30.

[30] O. Rubio, J. Herguido, M. Menéndez, Appl. Catal. A Gen. 272 (2004) 321–327.

[31] A. Talebizadeh, Y. Mortazavi, A.A. Khodadadi, Fuel Process. Technol. 90 (2009) 1319–1325.

[32] L. Zhang, F. Dumeignil, S. Paul, B. Katryniok, Appl. Catal. A Gen. 628 (2021) 118400.

[33] G. Kresse, J. Non. Cryst. Solids 192–193 (1995) 222–229.

[34] J.P. Perdew, K. Burke, M. Ernzerhof, Phys. Rev. Lett. 77 (1996) 3865–3868.

[35] D. Joubert, Phys. Rev. B - Condens. Matter Mater. Phys. 59 (1999) 1758–1775.

[36] F. Jing, B. Katryniok, F. Dumeignil, E. Bordes-Richard, S. Paul, J. Catal. 309 (2014) 121–135.

[37] A. Brückner, G. Scholz, D. Heidemann, M. Schneider, D. Herein, U. Bentrup, M. Kant, J. Catal. 245 (2007) 369–380.

[38] X. Cai, Y. Ma, Q. Zhou, Z. Zhang, W. Chu, W. Yang, React. Kinet. Mech. Catal. 133 (2021) 293-308.

[39] Y. Suchorski, L. Rihko-Struckmann, F. Klose, Y. Ye, M. Alandjiyska, K. Sundmacher, H. Weiss, Appl. Surf. Sci. 249 (2005) 231–237.

[40] F.P. Rouxinol, B.C. Trasferetti, R. Landers, M.A.B. De Moraes, 15 (2004) 324–326.

[41] J. Baltrusaitis, B. Mendoza-Sanchez, V. Fernandez, R. Veenstra, N. Dukstiene, A. Roberts, N. Fairley, Appl. Surf. Sci. 326 (2015) 151–161.

[42] J.K. Lee, V. Russo, J. Melsheimer, K. Köhler, R. Schlögl, Phys. Chem. Chem. Phys. 2 (2000) 2977–2983.